



Contents lists available at ScienceDirect

Remote Sensing of Environment

journal homepage: www.elsevier.com/locate/rse

Estimation of forest aboveground biomass in California using canopy height and leaf area index estimated from satellite data

Gong Zhang^{a,*}, Sangram Ganguly^a, Ramakrishna R. Nemani^b, Michael A. White^c, Cristina Milesi^d, Hirofumi Hashimoto^d, Weile Wang^d, Sassan Saatchi^e, Yifan Yu^f, Ranga B. Myneni^g

^a Bay Area Environmental Research Institute (BAERI)/NASA Ames Research Center, Moffett Field, CA 94035, USA

^b NASA Advanced Supercomputing Division, NASA Ames Research Center, Moffett Field, CA 94035, USA

^c Nature Publishing Group, San Francisco, CA, USA

^d Department of Science and Environmental Policy, California State University at Monterey Bay/NASA Ames Research Center, Moffett Field, CA 94035, USA

^e Jet Propulsion Laboratory, California Institute of Technology, Pasadena, CA 91109, USA

^f Department of Atmospheric and Ocean Sciences, University of California at Los Angeles, CA 90095, USA

^g Department of Earth and Environment, Boston University, MA 02215, USA

ARTICLE INFO

Article history:

Received 19 November 2013

Received in revised form 3 January 2014

Accepted 12 January 2014

Available online xxxx

Keywords:

Aboveground biomass

Leaf area index

Canopy height

Landsat

Uncertainty assessment

ABSTRACT

Accurate characterization of variability and trends in forest biomass at local to national scales is required for accounting of global carbon sources and sinks and monitoring their dynamics. Here we present a new remote sensing based approach for estimating live forest aboveground biomass (AGB) based on a simple parametric model that combines high-resolution estimates of leaf area index (LAI) from the Landsat Thematic Mapper sensor and canopy maximum height from the Geoscience Laser Altimeter System (GLAS) sensor onboard ICESat, the Ice, Cloud, and land Elevation Satellite. We tested our approach with a preliminary uncertainty assessment over the forested areas of California spanning a broad range of climatic and land-use conditions and find our AGB estimates to be comparable to estimates of AGB from inventory records and other available satellite-estimated AGB maps at aggregated scales. Our study offers a high-resolution approach to map forest aboveground biomass at regional-to-continental scales and assess sources of uncertainties in the estimates.

© 2014 Elsevier Inc. All rights reserved.

1. Introduction

Estimating and preserving the carbon stock in forests can help devise sequestration strategies and reduce emissions from deforestation and degradation (REDD) (Canadell et al., 2007; IPCC, 2007; Miles & Kapos, 2008; UNFCCC) as well as promote carbon credits to offset greenhouse gas emissions from other sources. Forest carbon stocks that change dynamically over time can be detected through periodic mapping of the total forest biomass (Baccini et al., 2012; Gurney & Raymond, 2008; Saatchi, Harris, et al., 2011; Saatchi, Marlier, Chazdon, Clark, & Russell, 2011). National inventories (e.g. the U.S. Forest Service Inventory and Analysis Program; FIA) provide the most detailed field estimates of forest biomass and disturbance history at national scale (Keith, Mackey, Berry, Lindenmayer & Gibbons, 2010). Although, methods for harmonizing forest inventory data are present at a national scale (McRoberts et al., 2009), the utility of such inventories for global-scale studies is limited because of national differences in measurement strategies, sparse sampling and out of date observations (Houghton, 2005). In addition, most inventories are designed to provide inferences only for administrative units or large regions. This is an important limitation because

reducing the uncertainty in emissions estimates requires spatially continuous measurements of forest carbon that are fine enough to capture the variability over a landscape that may undergo natural disturbances, succession or land-use changes.

Remote sensing allows mapping the aboveground portion of total forest biomass (AGB) over wide geographical extents, overcoming problems of field data underrepresentation (Gibbs, Brown, Niles & Foley, 2007; Lu, 2006; Saatchi, Houghton, Dos Santos Alvalá, Soares & Yu, 2007). Canopy reflectance measured by passive optical sensors and radar backscatter has been shown to correlate with field estimates of AGB densities (AGB value by instrument's footprint) (Foody, Boyd & Cutler, 2003; Steininger, 2000) but only up to densities of 300–400 Mg/Ha, after which the reflective measures show an asymptotic behavior with canopy closure (Saatchi et al., 2007). Space-borne LiDAR has improved the accuracy of the estimates of canopy vertical structure (Asner et al., 2010; Drake, Dubayah, Knox, Clark & Blair, 2002; Lefsky, Harding, Cohen, Parker & Shugart, 1999), but its sparse availability requires the fusion of multiple sources of data for large area mapping of AGB. Global forest height data estimated by the Geoscience Laser Altimeter System (GLAS; Harding & Carabajal, 2005), onboard the Ice, Cloud, and land Elevation Satellite (ICESat), have been combined with other remote sensing data (e.g. MODIS and ALOS PALSAR) and ground data aided with predictive models, to map the biomass density of forests across

* Corresponding author.

E-mail address: zhanggong07@gmail.com (G. Zhang).

large regions of the globe (Baccini, Laporte, Goetz, Sun & Dong, 2008; Boudreau et al., 2008; Goetz et al., 2009; Saatchi, Harris, et al., 2011; Saatchi, Marlier, et al., 2011). One limitation of this approach is that field data-driven model estimates of AGB have large uncertainties in regions where inventory data is absent and the inferences on under-sampled areas are usually based upon limited training data. Few studies have analyzed the theoretical linkages between remotely sensed vegetation indexes and biomass (Shi et al., 2013; Zhang & Kondragunta, 2006), which could advance the investigation of predictors and approaches for AGB estimation. In addition to coarse resolution mapping of biomass, there are increasing demands and attempts for estimating AGB density at finer resolution from Landsat reflectances (NASA's National Carbon Monitoring System Program; Avitabile, Baccini, Friedl & Schmullius, 2011; Lu et al., 2012) and other commercial satellites over continental-to-regional scales.

Uncertainty assessment is an essential component of AGB estimation based on remote sensing data because of the diversity in data sets involved, from satellite data to field-based samples and allometric models (Wulder et al., 2012). Because of differences in spatial resolution associated with field inventory plots, remotely sensed data, and the final AGB map, the sampling errors are difficult to assess through an error propagation approach (Mitchard et al., 2011). Many prediction models rely upon local data tuning, which causes the uncertainty of the experiment to vary depending on the data. To understand the contribution of each source of uncertainty in the AGB estimation, a general error propagation model is necessarily applied to a simple biomass estimation approach at uniform scale.

The objective of the study is to estimate AGB using a methodology based on the following premises:

- (a) We are able to integrate Landsat-estimated leaf area index (LAI) as a measurable structural attribute of canopy with forest height from GLAS to estimate a continuous height map using a simple parametric model at a spatial resolution of 30 m × 30 m;
- (b) We can estimate the AGB density from the continuous height map from (a) using a height-to-biomass functional relationship based on inventory data; and
- (c) We are able to estimate uncertainties for our AGB density due to errors in input data sources and model parameters using a Monte Carlo based error propagation model.

In the following sections we describe the region of study, data and methods used to estimate the AGB density, characterizing uncertainty in the final AGB product, and approaches to compare AGB density estimates with inventory based plot data and existing satellite-based AGB estimates. We estimate AGB using the computational facilities available at National Aeronautics and Space Administration (NASA) Earth Exchange (NEX) and thus refer to the biomass product as NEX-AGB. Our estimates of AGB density are comparable to Forest Inventory and Analysis (FIA) based AGB assessments and other satellite based estimates of AGB density at different aggregated scales (e.g. for counties and sub-ecoregions).

2. Data

2.1. Data for model construction

2.1.1. Land cover, elevation, and sub-ecoregion map

The study area for prototyping our methodology is the state of California, USA, which encompasses various eco-climatic zones with large variations in AGB. The National Land Cover Database (NLCD) 2006 provides accurate and consistent land cover information at a spatial resolution of 30 m × 30 m for the Conterminous United States (CONUS) and is an updated version of NLCD 2001 (WWW1). We used the NLCD 2006 map to select forested areas over California – the total forested land is approximately 9.54 million hectares, with evergreen forests comprising the majority in the

Sierra Nevada and the Pacific Northwest. The producer's accuracy for forest classes of NLCD 2006 was 94% for the continental United States (Wickham et al., 2013). In addition, we used a map of the ecological subregions of California with terminologies consistent with the FIA records and available at 1:500,000 to 1:1,000,000 scale from the US Forest Service (USFS) ECOMAP Team (WWW2). A total of 147 sub-ecoregions were used in our analysis. The National Elevation Dataset (NED) was used to verify the GLAS elevation estimates and generate slopes for height correction. Gesch (2007) reports that the root-mean-square error (RMSE) of NED is 2.44 m nationwide.

2.1.2. Landsat data

We used the USGS Global Land Survey (GLS) 2005 Landsat data for California (total of 45 cloud-free Landsat scenes). The GLS imagery consisted of both Landsat 5 and gap-filled Landsat 7 data at a spatial resolution of 30 m × 30 m with core acquisition dates from 2005 to 2006 (Gutman, Byrnes, Masek, Covington, Justice, Franks, & Headley, 2008; Gutman, Huang, Chander, Noojipady & Masek, 2013; WWW3). Each Landsat scene consists of a single day, mostly cloud-free acquisition, and the time of acquisition generally falls during leaf-on, peak of growing conditions for the location. Data recorded in 2004 and 2007 were used to replace GLS scenes with low image quality or excessive cloud cover. Over California, selecting images based on the peak of the growing season within the footprint of the Landsat scene results in spatial discontinuities once the scenes are mosaicked together (e.g. the growing season for crops near the San Francisco Bay Area peaks around April while the vegetation in adjacent scenes covering portions of the Sierra Nevada peaks later in the summer, in July or August). To rectify this issue, we harmonized the specific scenes to the same acquisition time (July–August) by replacing the April scenes with other cloud-free Landsat 5 scenes for July or August of the same year. If no Landsat 5 scenes were available during the GLS acquisition time, we chose scenes of the previous year or the year after. The harmonized mosaic of Landsat imageries has been previously used to map California LAI producing results comparable to the standard MODIS LAI product with error of 0.5 (Ganguly et al., 2012); however the remaining inconsistencies in acquisition dates of Landsat imageries contribute to uncertainty in the final AGB estimate.

2.1.3. GLAS canopy height

The Geoscience Laser Altimeter System (GLAS) staged in the Ice, Cloud, and land Elevation Satellite (ICESat) emits a 1064 nm laser pulse at an elliptical ground footprint of ~64 m diameter (Abshire et al., 2005), and the echo waveform of the laser pulse is recorded at the sensor system. The echo waveform data is referenced as the GLAS/ICESat L1A Global Altimetry Data (or GLA01). Associated with the GLA01 product is the GLAS/ICESat L2 Global Land Surface Altimetry Data (GLA14) product. GLA14 provides the geo-location of each footprint along with other parameters estimated from the waveform, such as the signal beginning and the echo energy peaks. In this study all the available GLA01 and GLA14 data with release version 3.1 for the time period from 2003 to 2007 were used to estimate the canopy height. Data after November 2007 were not used because of a decline in the laser power of the GLAS instrument (Lefsky, 2010).

2.1.4. Forest inventory data

The FIA Program of the USDA Forest Service measures and records information about forests at well designed ground plots (a standard FIA base plot includes roughly 1 sample location per 2400 ha). In this study, we gathered estimates of AGB, height, and the number of trees per area from the FIA database (FIADB - Version 4.0) for each plot within California (WWW4) for the time period from 2001 till 2007. A total of 2205 plots is available for California.

2.2. Data for accuracy assessment

To assess the accuracy of our biomass estimates, we compare three existing national AGB estimates against our NEX AGB estimate.

2.2.1. FIA AGB map

In addition to providing the plot samples, the FIA also summarizes the inventory plot data to report the status and trend of forest variables at state, county, and sub-ecoregions aggregated scale. The data are compiled for the time period from 2001 to 2009. We obtained the total AGB estimates at the county and sub-ecoregion levels by using the FIA Analysis EVALIDator tool with sampling error from 6.54% to 89.24% (referred to as FIA, WWW5).

2.2.2. NBCD AGB map

The Woods Hole Research Center has generated a high-resolution “National Biomass and Carbon Dataset for the year 2000” (referred to as NBCD) at a spatial resolution of $30\text{ m} \times 30\text{ m}$. The NBCD AGB estimation is based on an empirical modeling approach that combines USDA Forest Service FIA data with high-resolution InSAR data acquired from the 2000 Shuttle Radar Topography Mission (SRTM) mission and optical remote sensing data acquired from the Landsat ETM+ sensor (WWW6). Products from both the NLCD 2001 (land cover and canopy density) and LANDFIRE (WWW7, existing vegetation type) projects as well as topographic information from the USGS National Elevation Dataset (NED) are used within the NBCD AGB estimation as spatial predictor layers for canopy height and biomass. NBCD provides two biomass maps based on different allometric models. In our comparative analysis, we used the version of the NBCD map based on the Jenkins, Chojnacky, Heath and Birdsey (2003) height-to-biomass allometry. NBCD also reported biomass bootstrap validation of AGB estimates for two major forested zones in California ($r^2 = 0.27$, RMSE = 14.1 Mg/ha for coast redwood forests; $r^2 = 0.49$, RMSE = 10.1 Mg/ha for Sierra Nevada).

2.2.3. USFS AGB map

Blackard et al. (2008) provided a spatially explicit dataset of AGB (referred henceforth as USFS) by interpolating the FIA plot data mapping models through geospatial predictors. The predictors included the Moderate Resolution Imaging Spectrometer (MODIS)-estimated image band composites and percent tree cover, land cover proportions from the NLCD, topographic variables, monthly and annual climatic parameters, and other auxiliary variables (WWW8). The accuracy of USFS AGB is reported as r^2 at 0.53 and average absolute error at 163.1 Mg/ha in the Pacific Northwest (Blackard et al., 2008).

3. Methods

3.1. Estimating LAI from Landsat

Estimation of LAI requires surface spectral reflectances and land cover type as key input variables. We estimate the spectral surface reflectances from the Landsat GLS data using the Landsat Ecosystem Disturbance Adaptive Processing System (LEDAPS) atmospheric correction framework. Through the LEDAPS system, the raw data are calibrated to at-sensor radiance, converted to Top of Atmosphere (TOA) reflectance, and then atmospherically corrected using the MODIS/6S methodology (Masek et al., 2006). We estimate LAI from surface spectral reflectances for the forested pixels using a radiative transfer based inversion approach (Fig. 1a; Ganguly, Samanta, et al., 2008; Ganguly, Schull, et al., 2008; Ganguly et al., 2012; Appendix A). We also compute the normalized difference vegetation index (NDVI) from the Red and NIR surface spectral reflectance bands.

3.2. Estimating canopy height from GLAS data

The signal start of the GLAS-estimated echo waveform data detects the elevation of the uppermost surface of the canopy and the last signal peak is ideally attributed to the ground surface reflection (Harding & Carabajal, 2005). Canopy height was estimated over forested regions

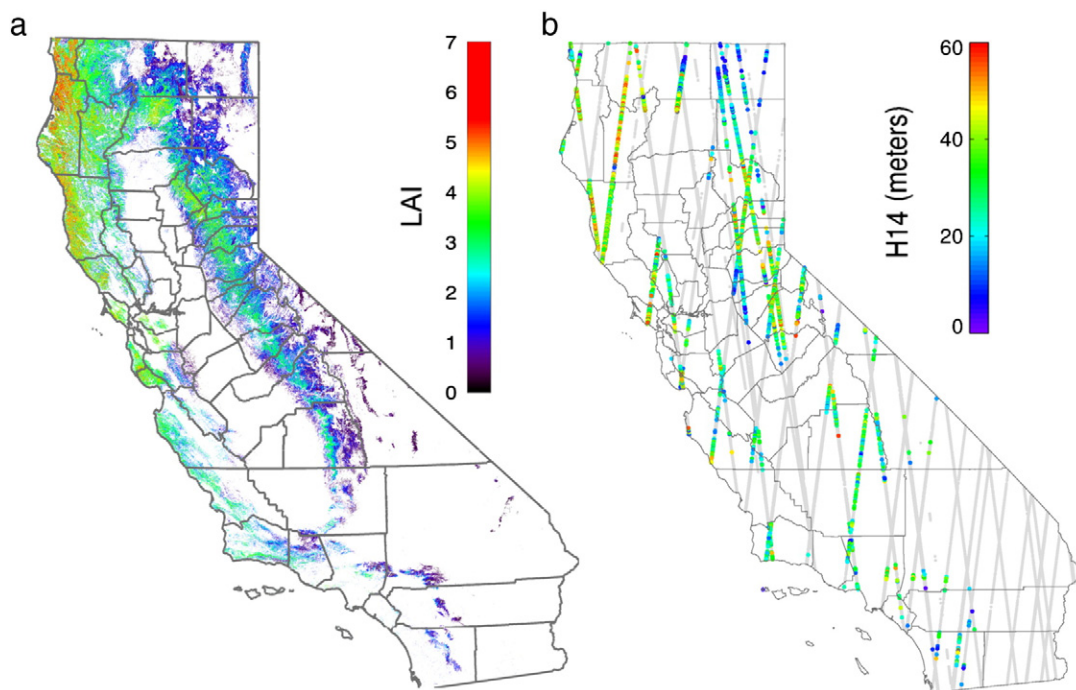


Fig. 1. (a) A $30\text{ m} \times 30\text{ m}$ Leaf Area Index map estimated from the Landsat Global Land Survey (GLS) 2005 data. (b) Geographic distribution of GLAS shots and estimated valid canopy height values in colors for the forested regions of California. (For interpretation of the references to color in this figure legend, the reader is referred to the web version of this article.)

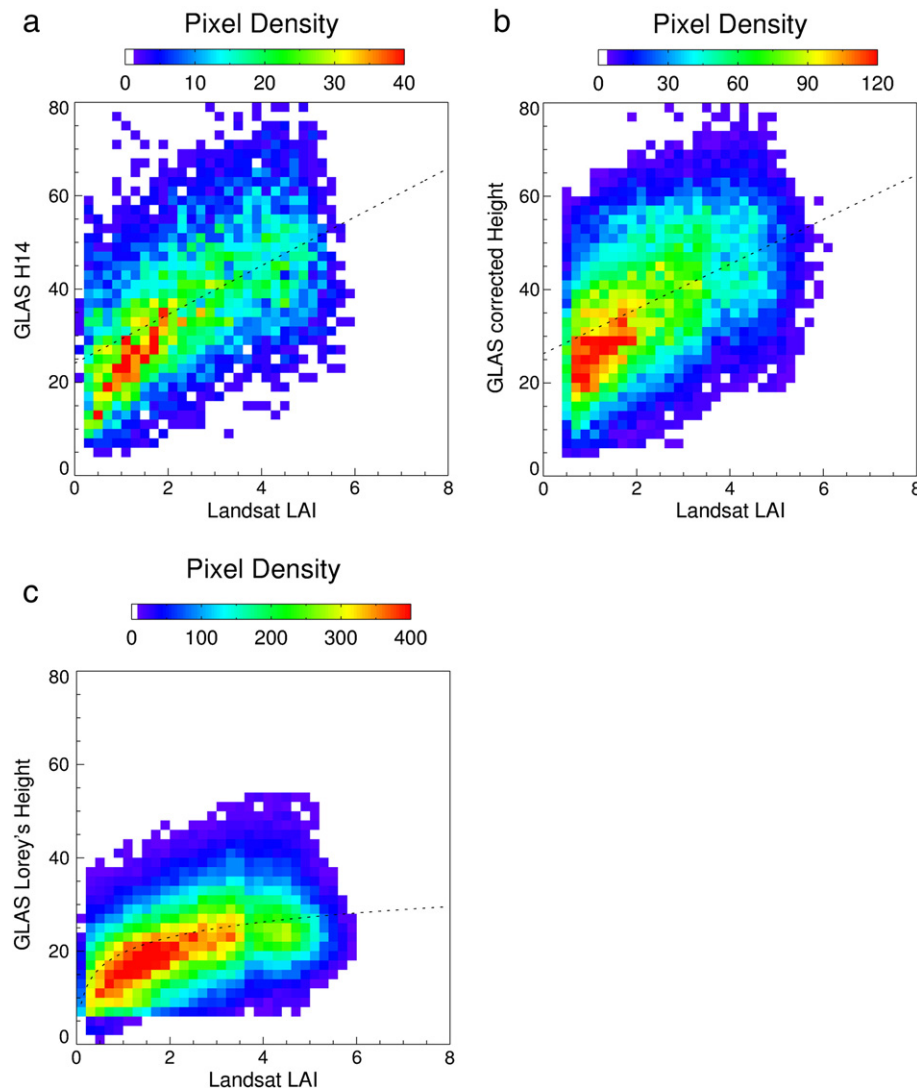


Fig. 2. (a) Density scatter plot between Landsat LAI and (a) GLAS maximum canopy height (H14); (b) GLAS slope corrected canopy maximum height (H0); (c) GLAS estimated Lorey's height. Bin size is 0.2 for LAI and 2 m for height, and dashed line shows the fitting model.

of California and the quality of the height estimates was assessed using accompanying GLAS data quality flags as well as auxiliary data from the National Elevation Data (NED) and Landsat (Appendix A).

The maximum canopy height on each footprint of GLAS plot is estimated as the distance between the signal start and the centroid of the ground peak recorded in GLA14 waveform data (we term as H14 from now onwards). This approach is only suitable for relatively flat surfaces where the echo waveform has a pronounced return from the ground surface compared to regions with rough topographical surfaces and high slopes (Sun, Ranson, Kimes, Blair & Kovacs, 2008). In order to establish the validity of the maximum canopy heights, H14 must be filtered by slope or corrected on non-flat plots. Some statistical correction methodologies based on ground data training are developed for specific forests (Chen, 2010; Lefsky, Keller, Pang, De Camargo & Hunter, 2007); however, physically based algorithms like the Geometric Optical-Radiative Transfer (GORT) model (Yang, Ni-Meister & Lee, 2011) are more feasible for consistent estimation of vegetation heights from GLAS data over large regions with different forest types.

The total number of GLAS shots for California during the growing season (May to October) from 2003 to 2007 amounts to 560,321, amongst which 40,793 are shots over pixels classified as forest by the NLCD 2006 map. With our strict signal quality filtering, described in Appendix A, the number of usable GLAS plots was reduced to 27,426

shots, which were further used to estimate the slope corrected maximum canopy height (H0) by using the GORT model slope correction algorithm (Yang et al., 2011). Moreover, by adding the slope filter, 8196 spatially representative shots remained for the calculation of the maximum canopy height (H14) (Fig. 1b). We defined the spatial representativeness by computing the mean distance from pixels classified as forests to the nearest GLAS shot. If the mean distance was large, the spatial representativeness was considered to be low, and vice versa (Hodgson et al., 2005). For all the 40,793 GLAS shots, the mean distance was 2.32 km, while for the valid shots (8196), the distance was computed as 2.30 km indicating that the slope-filtering of GLAS shots preserved the spatial representativeness of the dataset.

In addition to maximum canopy heights, we also used the statistically corrected GLAS-based canopy height – GLAS Lorey's Height – produced by Lefsky, 2010. GLAS Lorey's Height uses a larger dataset of GLAS shots (98,926 shots) from 2003 to 2009 by neglecting the effects of growing season and weak laser energy after 2007.

3.3. Mapping continuous height

GLAS height retrievals do not provide a spatially continuous coverage while the Landsat grid is a spatially continuous layer. We explore the relationship between GLAS height and LAI to extrapolate heights

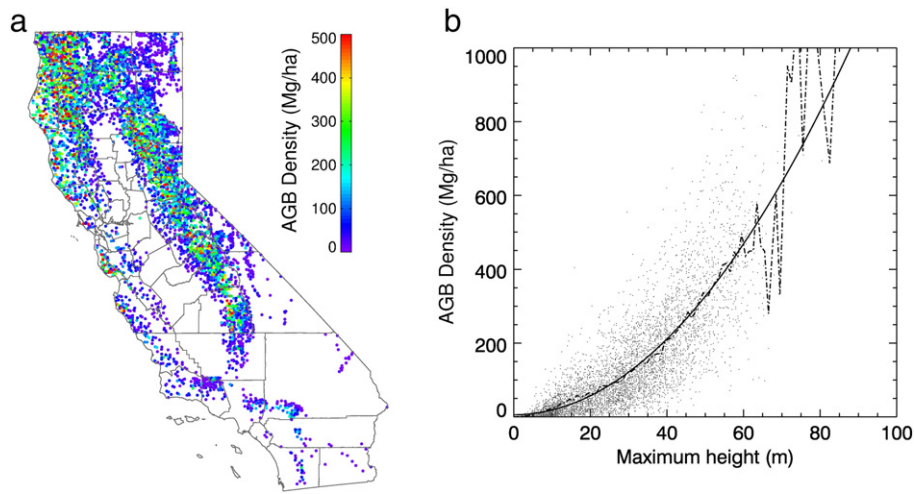


Fig. 3. (a) Plot level aggregated FIA aboveground biomass density estimates. (b) Relationship between height and aboveground biomass estimates for FIA plots (dotted line: bin average; and solid line: fitted model).

to pixels with a valid LAI. Field measurements and dynamic models show that different physiological traits of a forest, such as leaf area to tree height (h), are correlated with tree size following a power law (West, Brown & Enquist, 1999):

$$\text{LAI} \propto h^\alpha \quad (1)$$

where α regulates the polynomial degree of height. Based on a theoretical allometric model (Kempes, West, Crowell & Girvan, 2011), the power law between LAI and maximum tree height is a first order approximation that supports the assumption that we can obtain a near-linear relationship between Landsat estimated LAI and GLAS maximum canopy height (See Appendix A.). Differences in tree density across landscapes may blur this power law — e.g., in evergreen broadleaf forests significant canopy closure will result in measured signal saturation, which will affect the power law approximation. In general, the order of the power law between LAI and tree height shows variability around unity (e.g., Enquist, West & Brown, 2009 shows that LAI is proportional to $h^{0.72}$ in tropical regions). To explore relationships between leaf area and tree height for forests in California, we define the structural attributes of the forested pixels through (1) the LAI estimated from the Landsat 5 TM surface reflectance data and (2) the canopy height estimated from the available ICESat GLAS data.

A density scatter graph between the GLAS estimated maximum height (Fig. 1b) and Landsat LAI (Fig. 1a) nearest to the center coordinates of the GLAS shots shows a moderate but significant linear correlation ($r^2 = 0.27$, $p = 0.00$, RMSE = 12.33 m; Fig. 2a). In our study, we modeled the relationship between tree height and LAI for the conifer-dominated forests of California as:

$$\hat{H}_{14} = 24.10 + 5.22 \times \text{LAI}. \quad (2)$$

We also tested nonlinear relationships between height and LAI in discussion section (height as a function of LAI with different polynomial degrees) to demonstrate the effect of height in regulating the final AGB estimates.

We find a significant correlation between Landsat LAI and the slope-corrected H0 ($r^2 = 0.22$, p -value = 0.00; Fig. 2b). Besides the correlation coefficient value of LAI-H0 being slightly lower, the linear fitting parameters for LAI to H0 ($\hat{H}_0 = 26.26 + 4.80 \times \text{LAI}$) are similar to those for the fit of LAI to H14 (Eq. 2). The adjusted GLAS Lorey's height shows an even lower but still significant correlation to Landsat LAI ($r^2 = 0.18$, p -value = 0.00; Fig. 2c). GLAS Lorey's Height shows a notable saturation around height values of 20 m where LAI ranges from 2 to 6, indicating that LAI is a better estimator of canopy maximum

height than Lorey's height. In this study we estimated canopy maximum height based on a LAI to slope filtered H14 model. Since the fitting parameters in the LAI-H0 model are similar to ones used in the LAI-H14 model, we demonstrate the uncertainty assessment and direct comparison against the existing AGB map only for the LAI-H14 model.

3.4. Estimating the height-to-biomass functional relationship

We estimated a height-to-biomass functional relationship based on a total of 2205 FIA plots available over California for the period from 2000 to 2007 using information on tree size and FIA designed sample plots with different footprints (microplot, subplot, and macroplot). The average sampling area of FIA plots for California is $\sim 1146 \text{ m}^2$ as determined by the sampling area of each plot (approximately representing a square area of $34 \text{ m} \times 34 \text{ m}$ — similar to the spatial resolution of Landsat). The maximum and mean tree heights are estimated from all the trees available in each plot. The AGB density for a plot (AGBD_p) is the summation of individual tree biomass estimates weighted by a scalar factor, such that

$$\text{AGBD}_p = \sum_{i=1}^n \text{CARBONAG}_i \times \text{TPA}_i \times 2.0 \quad (3)$$

where n is the number of trees in each plot, CARBONAG_i is FIA estimated carbon in the aboveground portion of a tree by component ratio method (CRM) (Heath, Hansen, Smith, Miles & Smith, 2008), TPA_i is the species-specific scaling factor representing trees per area and 2.0 is a scalar factor to convert carbon to biomass in FIADB. The spatial representation of the FIA plot biomass density is shown in Fig. 3a. We estimated the relationship between maximum canopy height (H_{\max}) and AGB density (AGBD, Mg/ha) using the model specified in Lefsky et al. (2005). When using maximum heights the resulting model is

$$\text{AGBD} = 2.38 + 1.40 \times \hat{H}_{\max}^2 \quad (4)$$

with a r^2 of 0.64 and RMSE at 75.12 Mg/ha (Fig. 3b).

4. Accuracy assessment

4.1. Comparison with existing AGB estimates

We evaluated our AGB density estimates with field data and inter-compared them with other existing satellite-based biomass estimates

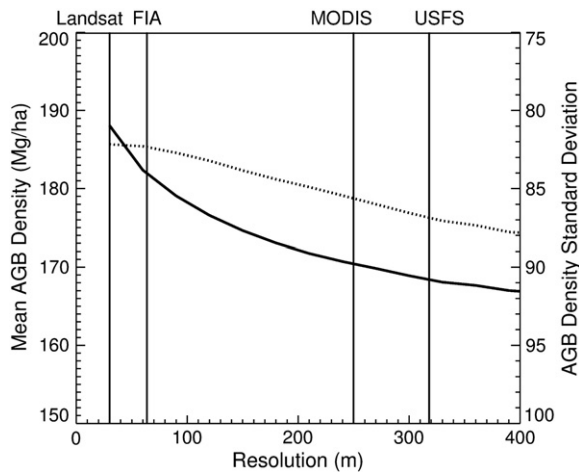


Fig. 4. Variation of NEX mean AGB density (solid line) and standard deviation (dotted line) with changes in spatial resolution.

(“USFS” and “NBCD”) aggregated by counties and sub-ecoregions. Total AGB estimates (measured in M ton) at the county and sub-ecoregion levels from the FIA Analysis EVALIDator tool were used as the standard against which to compare and validate the other estimates. FIA estimates include fewer sources of uncertainty (predominantly diameter and height measurement error and volume model prediction error), and the sample-based estimators used to calculate the large area estimates are assumed to have least bias. It is to be noted that all the estimates are based to some degree on the FIA ground measured data, therefore, the comparisons are not entirely independent.

It is important to note that plot- and pixel-level AGB density estimates are not directly comparable (Baccini, Goetz, Laporte, Sun & Dong, 2011) because AGB densities are inconsistent across spatial resolutions. As an example, we estimated the variation of AGB density with spatial resolution through an upscaling experiment by spatially aggregating our NEX 30 m × 30 m AGB density map for a region spanning the hardwood forests of Northern Sierra Nevada (covering an area of ~14,000 km²). We started with a majority resampling of the 30 m × 30 m NLCD land cover map to resolutions that are a factor of n (where $n = 1$ to 20). If an upscaled pixel at 60 m × 60 m resolution was identified as forest, we estimated the biomass density at this grid as the mean of the 4 corresponding 30 m × 30 m pixels. If the pixel is non-forest, the biomass value was set to zero. In this process, we estimated the mean and variance of estimated AGB density as well as the forest coverage for the whole region at different resolutions. Fig. 4 shows that the mean biomass density and the standard deviation of AGB density from the NEX map decreased monotonically at coarser resolutions, reaching ~10.6% at the USFS equivalent spatial resolution. The decreasing standard deviations of satellite-based AGB density estimates at coarser resolutions matches the pattern observed in field estimated AGB (Saatchi, Harris, et al., 2011; Saatchi, Marlier, et al., 2011). This upscaling exercise confirms the hypothesis that aggregating AGB density estimates across different spatial resolutions is theoretically incorrect and that estimates of AGB densities with different spatial resolutions cannot be directly compared. Comparisons can only be performed by aggregating the dataset to common spatial units.

In inter-comparing the maps, we estimated the total biomass at the county/sub-ecoregion level as:

$$AGB = \sum_{p=1}^n \hat{AGBD}_p \times Area \quad (5)$$

where $Area$ is the pixel area, \hat{AGBD}_p is the estimated biomass density at pixel, n is the number of forest pixels within the respective sub-

ecoregions based on the USFS sub-ecoregion map. The county total biomass was aggregated in a similar manner, except that in this case n is the number of forest pixels within the respective county.

4.2. Uncertainty modeling

In order to assess the uncertainty of our AGB density estimates from several sources, we classified the most likely error sources into following groups (Saatchi, Harris, et al., 2011; Saatchi, Marlier, et al., 2011):

- Forest coverage error ($\epsilon_{\text{coverage}}$) of NLCD 2006 map used in this study, given by accuracy of 94% reported for forest classification. The summation of pixel-level AGB estimates (Section 4.1, Eq. 5) by neglecting non-forest pixels introduces an uncertainty in the spatial aggregation of biomass, which has been estimated to be ~0.05% in the heavily forested Pacific Northwest (Blackard et al., 2008).
- Sampling error ($\epsilon_{\text{sampling}}$) associated with the representativeness of ground sampling plots and GLAS LiDAR shots to model the true distribution of AGB. Sampling error can be classified as (i) The standardized FIA plot sampling error is 3% per ~4000 km² forest, which produces a 0.5% error in the FIA data for all forests in California (WWW4). (ii) The sampling error associated with GLAS plots is assumed to be the same as that of the FIA plot, since the GLAS data have more plot numbers and the proximity of GLAS plots to forested pixels is similar to that of FIA (2.32 km compared to 1.85 km for FIA plots), even after strict filtering. The errors associated with differences in the spatial variability of GLAS and FIA plots and the AGB map are negligible because the area of the 30 m × 30 m pixel in the AGB map is approximately the same as the area of the footprint of FIA plots and/or GLAS LiDAR shots. We did not compute spatial sampling errors at the native resolution of the land cover map and Landsat and hence did not include them in our uncertainty model.
- Prediction error ($\epsilon_{\text{predict}}$) is the error associated with converting LAI to maximum canopy height and has several components: (i) error in LAI estimation from Landsat reflectances, which is approximately 0.5 LAI (Ganguly et al., 2012); (ii) error in estimating H14 from LAI in Eq. (2) ($r^2 = 0.27$, RMSE = 12.33 m); (iii) error associated with the conversion of H14 to FIA equivalent of H14 (H_{max}) – Chen (2010) reports this error over mountainous regions in California ($r^2 = 0.22$, RMSE = 9.12 m);
- Allometric error ($\epsilon_{\text{allometric}}$) which relates maximum canopy height to plot-level AGB estimate. This is due to (i) the error in FIA tree level AGB estimate based on CRM, whose accuracy is comparable to Jenkins et al. (2003; RMSE ≈ 0.2 log unit) for the dominant soft woods in California, and (ii) the error of the model from tree level to plot level in Eq. (4) ($r^2 = 0.64$, RMSE = 75.12 Mg/h). We also acknowledge the fact that there are uncertainties related to carbon-to-biomass factors, geo-rectification of FIA plots, and other FIA measurement errors in the height to biomass estimation model based on FIA ground measurements; however, FIA data bases do not report these uncertainties for individual FIA plots, and hence we exclude the sources of these uncertainties in the final uncertainty model.

In order to investigate the final uncertainty in our AGB estimates based upon the above mentioned factors, we implemented a Monte Carlo error propagation model to estimate the total prediction error for each pixel from four components by assuming all errors are independent and random (Heuvelink, 1999). Because our AGB estimation approach involves estimated data from different sources, we used a numerical error propagation approach such as a Monte Carlo stochastic simulation rather than an analytical approach like a Taylor expansion (Oksanen & Sarjakoski, 2005). We built a Monte Carlo approach with a random selection of 200 iterations in which the error range for each

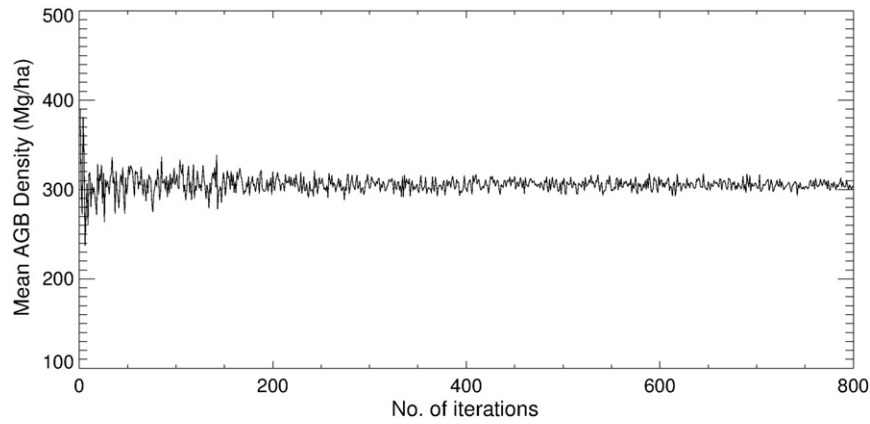


Fig. 5. NEX mean AGB density estimates as a function of iteration number in the Monte Carlo uncertainty assessment.

input variable and model are considered separately and then propagated them following the steps outlined below:

- 1) The LAI error ($\varepsilon_{\text{predict}_i}$) was first substituted in Eq. (2) with the model error ($\varepsilon_{\text{predict}_{ii}}$) to calculate the error associated with predicted H14, such that

$$\hat{H}14 = (24.10 + 5.22 * (\hat{LAI} + \varepsilon_{\text{predict}_i})) + \varepsilon_{\text{predict}_{ii}} \quad (6)$$

- 2) The uncertainty in the maximum canopy height, H_{max} is estimated incorporating errors associated with measured H14 ($\varepsilon_{\text{predict}_{iii}}$), predicted H14 (Eq. 6), and the GLAS sampling error ($\varepsilon_{\text{sampling}_{ii}}$), such that

$$\hat{H}_{\text{max}} = \hat{H}14 + \varepsilon_{\text{predict}_{iii}} + \varepsilon_{\text{sampling}_{ii}} \quad (7)$$

- 3) The uncertainty in pixel-level AGB is estimated by incorporating the allometric uncertainties, the FIA sampling error ($\varepsilon_{\text{sampling}_i}$), and the forest coverage uncertainty ($\varepsilon_{\text{coverage}}$) in Eq. (4), such that

$$\hat{AGB} = 2.39 + 0.14 \times \hat{H}_{\text{max}}^2 + \varepsilon_{\text{allmetric}_i} + \varepsilon_{\text{allmetric}_{ii}} + \varepsilon_{\text{sampling}_i} + \varepsilon_{\text{coverage}} \quad (8)$$

Finally, the pixel-level AGB uncertainty was calculated in terms of RMSE,

$$\sigma_{\hat{AGB}} = \sqrt{\frac{\sum_{i=1}^n (\hat{AGB}_i - \hat{AGB})^2}{n}} \quad (9)$$

where n is set as 200 – the mean value of AGB estimates stabilizes after 200 iterations as shown in Fig. 5.

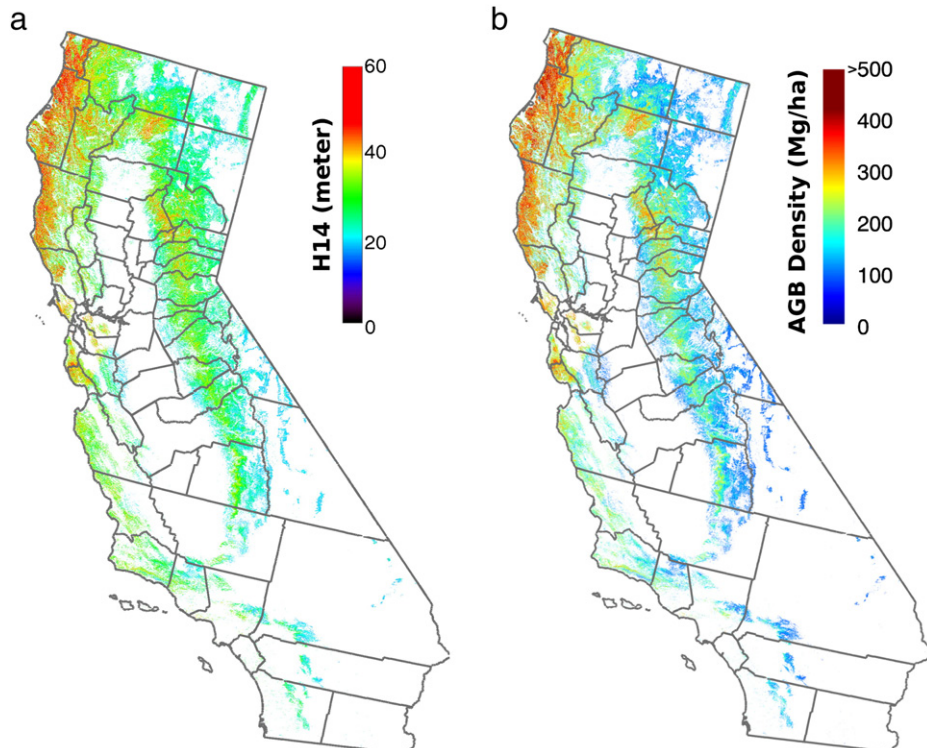


Fig. 6. (a) Continuous maximum canopy height estimated using the linear model fit relationship between H14 and Landsat LAI. (b) AGB density estimates at 30 m × 30 m spatial scale.

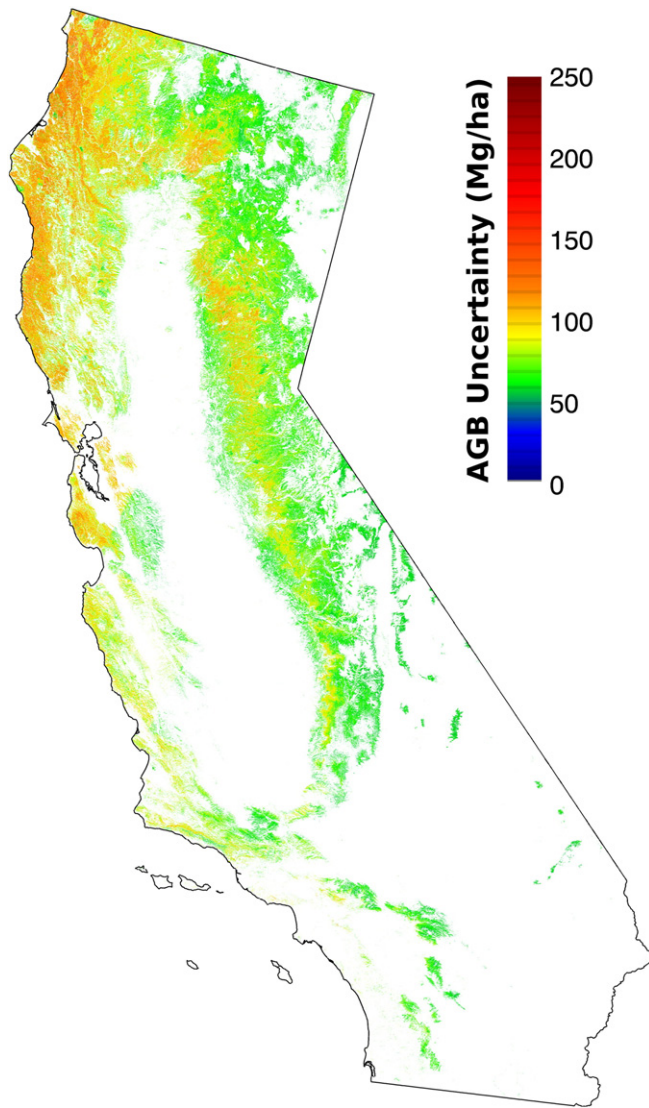


Fig. 7. AGB uncertainty (RMSE) for all pixels.

5. Results

Capitalizing on the statistical correlation between LAI and maximum height (Section 3.3), we used the linear model from Fig. 2a to estimate height values (Fig. 6a) for the remaining $30 \text{ m} \times 30 \text{ m}$ forested pixels after slope and quality filtering from LAI. Live forest AGB density (Fig. 6b; referred to as “NEX”) was estimated from the resulting continuous maximum height fields (Fig. 6a) at a $30 \text{ m} \times 30 \text{ m}$ spatial resolution using the height-to-biomass functional relationship as estimated in Section 3.4. The AGB density estimates ranged from 100 Mg/ha at sparse forests to over 500 Mg/ha in coast redwood forests.

The results from the error propagation model suggest that the uncertainty of AGB estimates ranges from 40 Mg/ha (for low AGB density) to 150 Mg/ha (for high AGB density) as RMSE at the pixel level (Fig. 7), and it is constrained to less than $\pm 40\%$ for the entire range of AGB. It is worth to note that the uncertainty values are the lower bounds of our uncertainty assessment since multiple sources of uncertainty were not considered in our analysis (c.f. Section 4.2).

To compare existing satellite-based AGB maps, we estimated the total aboveground biomass values for counties and sub-ecoregions within California as described in Section 4.1. The range in total AGB amongst county and sub-ecoregions is remarkably large, ranging from less than 0.1 M ton to greater than 200 M ton (Fig. 8). Fig. 9a shows notable disagreements among the frequency distributions of the satellite-based AGB density estimates compared at their native resolutions. Pixel-level variations in AGB density estimates arise mainly from spatial resolution-dependent changes in forested fractions of the pixels, which can be ascribed to the scaling effects shown in Fig. 4. The mean AGB density estimate of all pixels in the NBCD map is 212.4 Mg/ha, followed by NEX at 201.2 Mg/ha and USFS at 174.2 Mg/ha. The standard deviations of the estimates amount to 93.38 Mg/ha (NBCD), 73.60 Mg/ha (NEX), and 86.05 Mg/ha (USFS). When comparing the FIA total biomass estimates with the satellite-based estimates for all the counties and sub-ecoregions present in our study region (Fig. 9b, Fig. 9c, and Table 1), NEX shows the least RMSE (~ 8.63 M ton for county total and ~ 8.38 M ton for sub-ecoregions) compared to the FIA estimates. A comparison of the differences between the various remote sensing based AGB estimates and the FIA estimates for each sub-ecoregion and county is shown in Fig. 10 and Table 1.

We analyze the differences in spatial patterns of aggregated AGB estimates by stratifying the ecoregions and sub-ecoregions by biomass

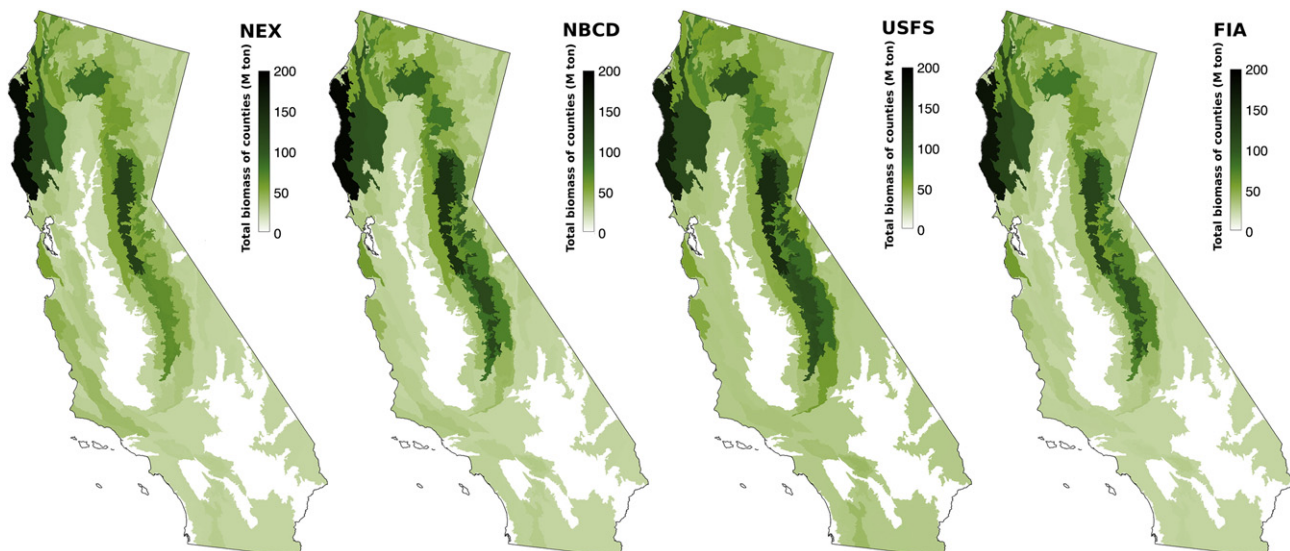


Fig. 8. Total AGB (in M ton) estimates at sub-ecoregion level from the NEX, NBCD, USFS and FIA AGB density maps.

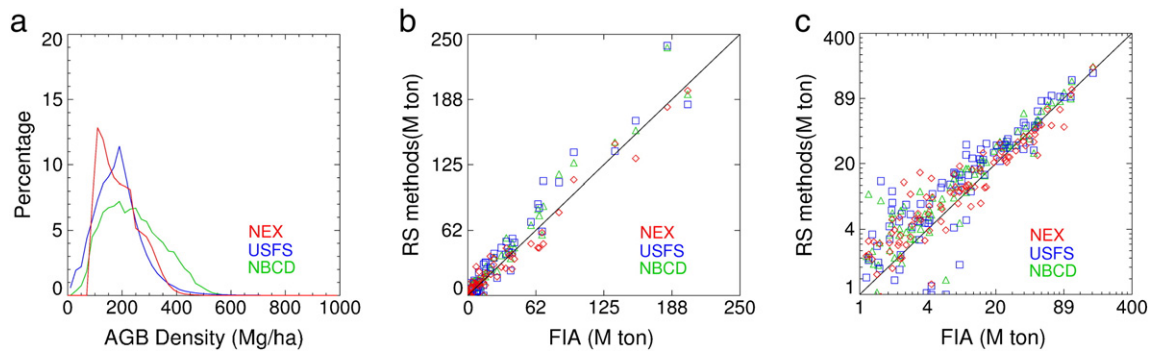


Fig. 9. Evaluation of AGB estimates for forested regions in California. (a) Frequency distribution of AGB density estimates from NEX, USFS and NBCD. (b) Comparison of satellite-based aggregated estimates of total AGB and FIA estimated total AGB for counties. (c) Similar comparison as (b) but for sub-ecoregions is presented in a log scale to elucidate lower dynamic range of AGB.

class intervals and calculating total biomass estimates and their deviation from the FIA estimates in terms of relative difference, r^2 , RMSE and percentage accuracy (Tables 2 and 3). Most forests in California are located in five ecosystem provinces (Table 2) representing 99.1% of the total forest AGB estimates. The NEX total AGB estimates compare best to the FIA estimates for the dominant forested ecosystem provinces (M261 and M263 encompass approximately 50% of the total area of the sub-ecoregions) while they show a larger difference with regard to FIA estimates for the rest of the sub-ecoregions. To supplement the analysis further, Table 3 provides r^2 , RMSE, and percentage accuracy for sub-ecoregions grouped by total biomass ranges, illustrating the disparities that can be seen when we go from low to high biomass. The RMSE of different AGB maps compared to FIA increases when pooling all the sub-ecoregions together. However, the percentage accuracy improves if we consider only the sub-ecoregions with higher biomass (>10 M ton). The correlation coefficient and percentage accuracy are lower when we pool sub-ecoregions that cover the intermediate (1 to 10 M ton) and lower biomass ranges (<1 M ton).

In terms of accuracy, most of the satellite-based total AGB are close to FIA (10%–30% difference) for sub-ecoregions with more than 4.5 M ton of biomass, with the NEX showing higher accuracy. In the lower biomass category (<4.5 M ton), USFS shows the least mean error. Overall, the number of sub-ecoregions that show an agreement in total AGB with FIA is highest for NEX followed by NBCD and USFS in term of RMSE (Table 1 and Fig. 9c).

6. Discussion

The simple model discussed in this paper is suitable to be applied on other forest types with sparse field data. Limitations in our approach may result from input data availability and uncertainty as well as accuracy of the models. Errors in the input data (Landsat and GLAS acquisitions) caused by atmospheric contamination and saturation of pixel-estimated surface reflectances might increase the uncertainty of our model. The auxiliary input data uncertainties (e.g. NLCD, NED, FIA plot data, FIA allometric model) also contribute to the final AGB uncertainty. The models estimating AGB from height via LAI also lead to a large

amount of uncertainty where the correlation between these variables is moderately low. This is the case of dense canopies, where RMSE is larger than 100 Mg/ha. Additionally, the spatial aggregation of biomass in Eq. (5) through the summation of AGB over only pixels classified as forest introduces an uncertainty of omission. Assuming that the uncertainties from different sources are independent, we implemented a Monte Carlo based uncertainty assessment. Among the numerous sources contributing to errors, we discuss some essential elements excluded in our uncertainty model.

The algorithm for the estimation of the LAI used in this study is a source of uncertainty and perhaps more so the population of standing vegetation over which LAI is being estimated. The Landsat measures of reflectance from which LAI is calculated are sensitive to the density of the standing trees and ground vegetation. The uncertainty associated with LAI is non-linear over its range of estimation and differs by forest types. Detailed descriptions of species and forest types are helpful to understand the relationship between height and LAI and in identifying additional factors contributing to uncertainties associated with LAI. However, the variability in uncertainty estimates is difficult to quantify and thus in this study we make a conservative assumption of uniform deviations in the LAI estimates.

In this study we applied a single linear model (1st order polynomial) between H14 and LAI, although theoretically, the power law between leaf area and tree height varies amongst forest types. In order to demonstrate the effect of models of different polynomial degrees, we computed the county level mean biomass uncertainty (averaging the pixel level AGB density uncertainty values within the specific county) for different values of α in Eq. (1). Fig. 11 shows the county and sub-ecoregion average percent uncertainty with respect to total biomass at $\alpha = 0.5, 1, 1.5$, and 2, which translates to height as a function of $LAI^{0.5}$, $LAI^{1.5}$, and LAI^2 . We found that for $\alpha = 1$ the uncertainties were constrained within 0–20% of the total biomass estimated from averaging the pixel AGB density estimates, while the percent uncertainty was larger for low values of total biomass and decreased for values of high total biomass. This exercise also showed that the uncertainty in the AGB estimates can be constrained at county and sub-ecoregion level but will vary depending on the spatial scale at which it is reported. This observation agrees

Table 1

Correlation coefficients and RMSE $\left(\sqrt{\frac{\sum_i (RS_i - FIA_i)^2}{N}} \right)$ for county and sub-ecoregion total biomass estimated from FIA and remote sensing estimated maps, where RS refers to NEX/NBCD/USFS estimates.

Metrics (w.r.t. FIA)	NEX	NBCD	USFS
<i>County</i>			
r^2	0.963	0.965	0.944
RMSE (M ton)	8.63	11.60	14.17
<i>Sub-ecoregion</i>			
r^2	0.940	0.966	0.938
RMSE (M ton)	8.38	9.11	11.30

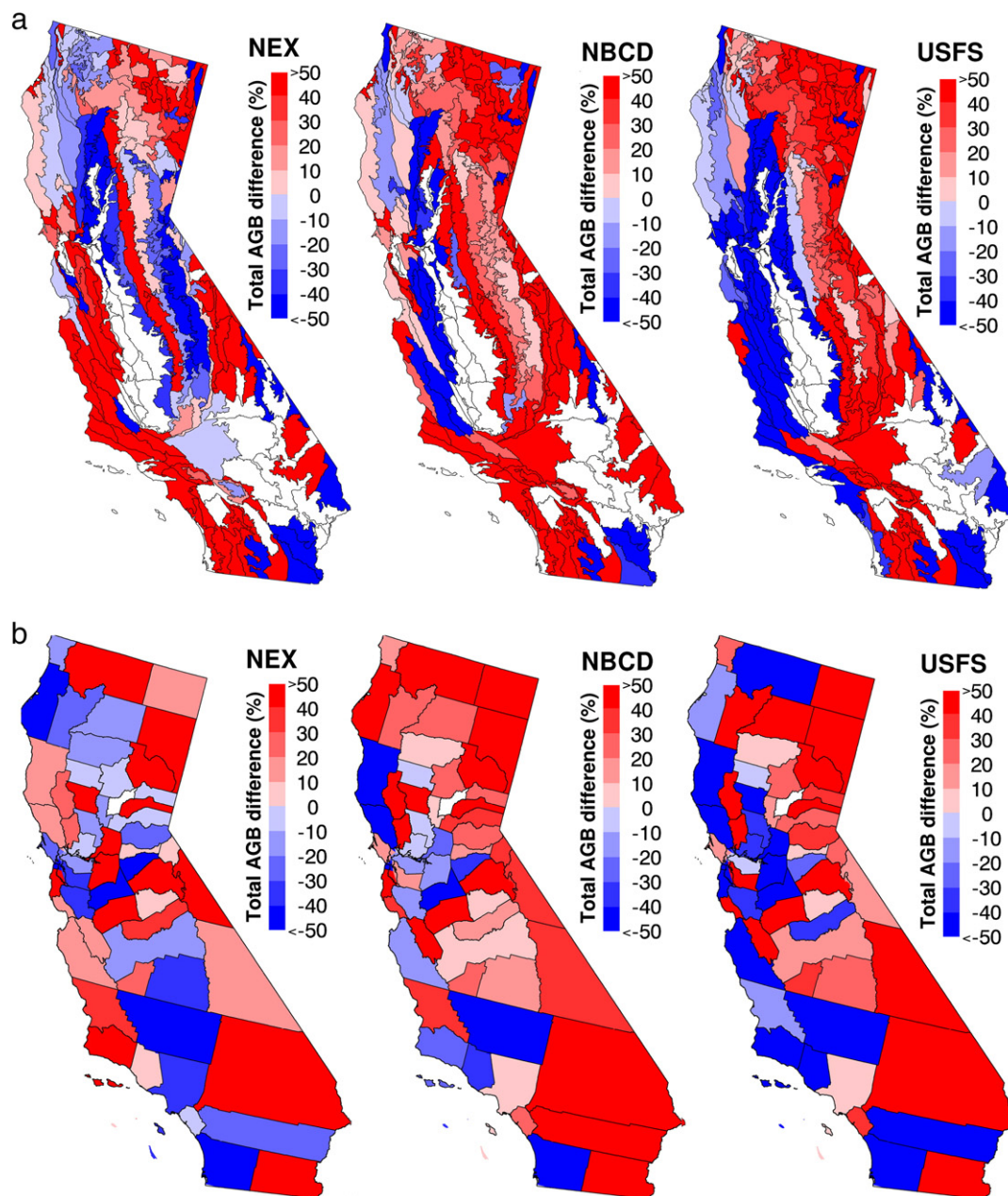


Fig. 10. (a) Difference between the satellite and the FIA total AGB estimates by sub-ecoregion. (b) Same as (a) but by counties.

with the previous findings that showed less uncertainty in AGB estimates when aggregating the data over larger regions (Saatchi, Harris, et al., 2011).

Alternative slope correction methods based on auxiliary topographic data could largely benefit the accuracy of forest height estimations in complex terrains. Although a relatively large number of GLAS shots remain after external slope filtering, a topographic/geometric correction of GLAS-estimated canopy height would increase the number of samples at sloped locations and thus the representativeness of non-flat terrains. While the relationship between LAI and slope-corrected H_0 was similar to that of slope-filtered LAI- H_{14} model obtained in this study, future efforts of exploring alternative slope correction methods may improve the estimation of height values for forests in mountainous regions.

The Landsat pixel has the approximate footprint area of a GLAS shot and FIA plot but a different shape. Assessments of the uncertainty associated with shape differences will be the object of future investigations carried out over a small region with high resolution measurements.

NEX AGB maps the biomass of California for the nominal year 2005. Although most remotely sensed predictors were acquired around the year 2005 (e.g., NLCD 2006, GLS 2005, GLAS 2003–2007), an additional source of uncertainty arises from temporal factors such as short-term forest disturbance and land cover change.

Although this study and other validation analyses of biomass (Nelson, Short & Valenti, 2004; Pflugmacher, Cohen, Kennedy & Lefsky, 2008) consider FIA-estimated AGB a fiducial marker, it is important to note that the FIA-estimated AGB at tree level is not measured directly but is based on species-specific allometric models. In addition to intrinsic uncertainties tied to FIA tree and plot-level AGB estimates, there are errors associated with scaling FIA estimates to larger spatial units such as counties/sub-ecoregions. The spatial pixel underrepresentation is introduced into regional AGB estimates by differences in the number of FIA plot samples per county/sub-ecoregion (most counties/sub-ecoregions have no less than 20 FIA plot samples, but there are sub-ecoregions which have more than hundred FIA plots). Airborne LiDAR estimates of AGB at a fine spatial resolution could serve as a potential validating kernel linking

Table 2

Total biomass estimates (in M ton) and relative difference between total biomass and FIA estimates (in parenthesis) by ecoregion for California. The relative difference is calculated as $((RS - FIA) / FIA) \times 100$.

Ecoregion province (no. of sub-ecoregions)	NEX	NBCD	USFS	FIA
M261 (67)	1270.3 (−8.0%)	1652 (19.6%)	1760 (27.5%)	1381
263 (7)	282.7 (0.3%)	273.5 (−2.9%)	235.4 (−16.4%)	281.7
261 (14)	110.3 (57.8%)	93.5 (33.8%)	53.9 (−23.0%)	69.9
M262 (22)	98.3 (82.9%)	63 (16.8%)	66 (24.3%)	54
262 (6)	1.2 (−76.6%)	6.3 (23.1%)	0.1 (−98.5%)	5.1
Others (31)	24.4 (50.0%)	59.62 (221.4%)	37.8 (145.1%)	15.4

Table 3

Sub-ecoregion total AGB difference between remote sensing methods and FIA for three broad class ranges are reported in the percentage accuracy $\left(\frac{1}{N} \sum_{i=1}^N \frac{(RS_i - FIA_i)}{FIA_i} \times 100\right)$ in addition to RMSE and r^2 .

Total biomass range (M ton)	Number of sub-ecoregions	NEX	NBCD	USFS
r^2				
<4.5	41	0.05	0.03	0.01
4.5–20	54	0.42	0.36	0.25
>20	52	0.91	0.95	0.90
RMSE(M ton)				
<4.5	41	2.89	2.07	2.83
4.5–20	54	4.44	4.90	7.71
>20	52	12.2	11.62	13.54
Accuracy (%)				
<4.5	41	190.5	296.2	83.2
4.5–20	54	19.2	23.6	32.6
>20	52	−8.8	15.2	14.5

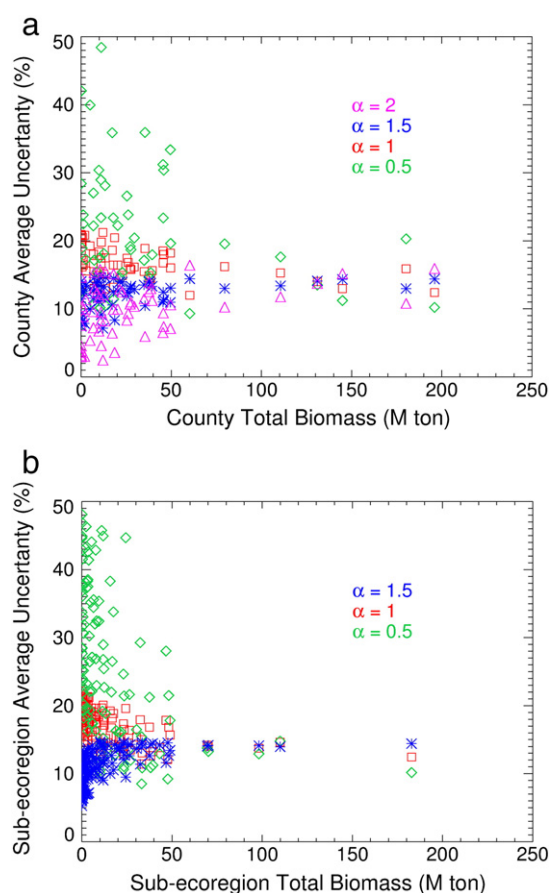


Fig. 11. (a) County and (b) sub-ecoregion average uncertainty as a function of total AGB for different values of α (α is defined in Eq. 1).

field measurements to large scale AGB estimates; however, such maps estimated at fine resolution with limited spatial coverage may be inadequate for validating AGB values over large regions. For this study we consider only FIA-based estimates as benchmark.

Another possible explanation for the disagreement in AGB estimates is the definition and extent of forested land within the sub-ecoregions (this refers to the differences in forested area estimates at different spatial resolution which in turn introduces the disparities seen in AGB density estimates). Last but not least, some sources and estimators such as FIA plot and tree level AGB in our model have larger uncertainties than the estimates in results, a problematic issue raised by Stehman (2009).

7. Conclusion

The results from this study are in support of the ongoing activities of NASA's National Carbon Monitoring System Program to help devising data fusion strategies for high spatial resolution AGB estimation over large regions. We found that Landsat LAI is significantly related to several GLAS height metrics, which implies that the Landsat LAI is a valuable AGB predictor. This study provides a methodology to estimate live AGB at a sufficiently high spatial resolution (30 m \times 30 m) based on a simple parametric model. Our model builds upon the premise that high-resolution estimates of LAI and canopy maximum height can be used to estimate AGB independently of *a priori* field data training and with a limited uncertainty assessment. In an effort to validate the final AGB estimates, we enumerate ways to compare available AGB density maps at different spatial resolutions and FIA inventory data. Results show that at an aggregated scale, our AGB estimates are comparable to the inventory-based estimates and available satellite-based estimates.

It should be noticed again that our simple model of estimating AGB from remotely sensed data implies uncertainties related to the remote sensing data itself, model construction, and sampling, some of which were neglected in this study. This preliminary study provides AGB

estimates at 30 m × 30 m resolution, these are associated with many uncertainties and the regional aggregation of AGB is more reliable.

Acknowledgements

We acknowledge funding from the Carbon Monitoring System (CMS) program at NASA. We thank the anonymous reviewers and editors for their constructive comments and edits to the manuscript. We are particularly grateful to Dr. Ronald E. McRoberts for all his critical inputs in improving the manuscript. This research was performed using the NASA Earth Exchange (NEX) computing facilities.

Appendix A1. Estimating Landsat LAI

Landsat surface reflectances estimated from the TOA reflectances by the atmospheric correction routine assume that the target is Lambertian and infinite and that the gaseous absorption and particle scattering in the atmosphere can be decoupled. The auxiliary data used in the processing chain include gridded TOMS (Total Ozone Mapping Spectrometer) data, column water vapor from the National Oceanic and Atmospheric Administration (NOAA) National Centers for Environmental Protection (NCEP) reanalysis data, digital topography and NCEP surface pressure data. The dark, dense vegetation (DDV) type method is used to extract the atmospheric optical depth (AOD) directly from the imagery (Kaufman et al., 1997). Based on the physical correlation between chlorophyll absorption and liquid water absorption, this method hypothesizes a linear relation between the shortwave-infrared (2.2 μm) surface reflectance (nearly unaffected by the atmosphere) and surface reflectance in the visible bands (Masek et al., 2006). The specific relations are estimated from an analysis of data from Aerosol Robotic Network (AERONET) sites where AOD is measured directly (WWW8). The output from the LEDAPS provides surface spectral reflectances for all the available spectral bands with corresponding quality assurance (QA) flags for clouds, missing data, and an aerosol optical thickness map for the blue band.

We estimate LAI from surface spectral reflectances for the forested pixels using a radiative transfer based inversion approach (Fig. 1a; Ganguly, Samanta, et al., 2008; Ganguly, Schull, et al., 2008; Ganguly et al., 2012). The algorithm provides a computationally efficient way of parameterizing the Bidirectional Reflectance Factor (BRF) as a function of spatial resolution and wavelength. A reflectance model inversion is performed and operated through minimizing a merit function, which yields an estimate of LAI by minimizing the summed differences between simulated and measured reflectances for the Red, NIR and SWIR bands (Ganguly et al., 2012).

2. GLAS shots filtering

2.1. GLAS signal quality filtering

- The seasonal time period from May to October for each year is used as a first level screening of GLAS shots to best approximate the growing season.
- To avoid factors pertaining to atmospheric forward scattering and signal saturation, only the cloud-free (flag corresponding to FRir_qaFlag = 15 in the GLA14 product) and saturation-free (i.e. saturation index satNdx = 0 in the GLA14 product) shots were considered.
- A data filter was applied to make sure that the difference in elevation of the ground peak estimated from the waveform and the ground elevation estimated from the 30 m × 30 m National Elevation Dataset (NED) data is less than 100 m, which is far beyond the NED valid range.
- The 30 m × 30 m NLCD 2006 map is used to delineate forest versus non-forest pixels. The center location of the GLAS shot with the

nearest NLCD pixel center coordinate is matched to classify the GLAS shot as either non-forest or forest.

- Using the Landsat spectral band data, a threshold RED spectral reflectance value of 0.3 is further used to filter non-vegetated pixels. This step is particularly useful for detecting regions or pixels that have forest misclassification errors as introduced from the NLCD map.

2.2. Slope filtering

Additional filtering is performed by using the terrain slope gradient information calculated from the NED 30 m × 30 m elevation data. A 3×3 slope gradient kernel centered over each 30 m × 30 m pixel is calculated. The center location of the GLAS shot with the nearest slope gradient pixel is matched to perform the filtering. If the slope gradient value is 0.5 and higher, the nearest GLAS shot is excluded from the analysis.

3. Theoretical linkage between LAI and height

Field measurements and dynamic models show that different physiological traits of a forest are correlated with tree size following a power law. Based on a simple allometric model (West et al., 1999), the total leaf area is proportional to maximum tree height (h) such that:

$$a_l * (n^N) \propto h^3 \quad (\text{A1})$$

where a_l is the leaf area for each leaf, n^N is the number of leaves, and the product of them represents the total leaf area. Niklas and Spatz (2006) provide another relationship between canopy radius and maximum tree height such that:

$$r_{\text{can}} \propto h \quad (\text{A2})$$

where r_{can} is the canopy radius.

Since LAI is the total leaf area divided by projected canopy area, using the proportionality rules from Eqs. (1) and (2), we can relate LAI with maximum height (Kempes et al., 2011) as:

$$\text{LAI} = \frac{a_l * n^N}{\pi * r_{\text{can}}^2} \propto \frac{h^3}{\pi * h^2} \quad (\text{A3})$$

The power law between LAI and maximum tree height is a first order approximation that supports the assumption that we can obtain a near-linear relationship between Landsat estimated LAI and GLAS maximum canopy height. Differences in tree density across landscapes may blur this power law – e.g., in evergreen broadleaf forests, significant canopy closure will result in measured signal saturation which will affect the power law approximation. In general, the order of the power law between LAI and tree height shows variability around unity (e.g. Enquist et al., 2009 shows that LAI is proportional to $h^{0.72}$ in tropical regions).

References

- Abshire, J. B., Sun, X., Riris, H., Sirota, J. M., McGarry, J. F., Palm, S., et al. (2005). Geoscience laser altimeter system (GLAS) on the ICESat Mission: On-orbit measurement performance. *Geophysical Research Letters*, 32(21).
- Asner, G. P., Powell, G. V. N., Mascaro, J., Knapp, D. E., Clark, J. K., Jacobson, J., et al. (2010). High-resolution forest carbon stocks and emissions in the Amazon. *Proceedings of the National Academy of Sciences*, 107(38), 16738–16742.
- Avitabile, V., Baccini, A., Friedl, M.A., & Schmullius, C. (2011). Capabilities and limitations of Landsat and land cover data for aboveground woody biomass estimation of Uganda. *Remote Sensing of Environment*, 117, 366–380.
- Baccini, A., Goetz, S. J., Laporte, N., Sun, M., & Dong, H. (2011). Reply to Comment on "A first map of tropical Africa's above-ground biomass derived from satellite imagery". *Environmental Research Letters*, 6, 049002.
- Baccini, A., Goetz, S. J., Walker, W. S., Laporte, N. T., Sun, M., Sulla-Menashe, D., et al. (2012). Estimated carbon dioxide emissions from tropical deforestation improved by carbon-density maps. *Nature Climate Change*, 2.3, 182–185.

- Baccini, A., Laporte, N., Goetz, S. J., Sun, M., & Dong, H. (2008). A first map of tropical Africa's above-ground biomass derived from satellite imagery. *Environmental Research Letters*, 3, 045011.
- Blackard, J. A., Finco, M. V., Helmer, E. H., Holden, G. R., Hoppus, M. L., Jacobs, D.M., et al. (2008). Mapping U.S. forest biomass using nationwide forest inventory data and moderate resolution information. *Remote Sensing of Environment*, 112(4), 1658–1677.
- Boudreau, J., Nelson, R. F., Margolis, H. A., Beaudoin, A., Guindon, L., & Kimes, D. S. (2008). Regional aboveground forest biomass using airborne and spaceborne LiDAR in Quebec. *Remote Sensing of Environment*, 112(10), 3876–3890.
- Canadell, J. G., Le Quéré, C., Raupach, M. R., Field, C. B., Buitenhuis, E. T., Ciais, P., et al. (2007). Contributions to accelerating atmospheric CO₂ growth from economic activity, carbon intensity, and efficiency of natural sinks. *Proceedings of the National Academy of Sciences*, 104(47), 18866.
- Chen, Q. (2010). Retrieving vegetation height of forests and woodlands over mountainous areas in the Pacific Coast region using satellite laser altimetry. *Remote Sensing of Environment*, 114(7), 1610–1627.
- Drake, J. B., Dubayah, R. O., Knox, R. G., Clark, D. B., & Blair, J. (2002). Sensitivity of large-footprint lidar to canopy structure and biomass in a neotropical rainforest. *Remote Sensing of Environment*, 81, 378–392.
- Enquist, B. J., West, G. B., & Brown, J. H. (2009). Extensions and evaluations of a general quantitative theory of forest structure and dynamics. *Proceedings of the National Academy of Sciences*, 106(17), 7046–7051.
- Foody, G. M., Boyd, D. S., & Cutler, M. E. (2003). Predictive relations of tropical forest biomass from Landsat TM data and their transferability between regions. *Remote Sensing of Environment*, 85(4), 463–474.
- Ganguly, S., Nemani, R. R., Zhang, G., Hashimoto, H., Milesi, C., Michaelis, A., et al. (2012). Generating global Leaf Area Index from Landsat: Algorithm formulation and demonstration. *Remote Sensing of Environment*, 122, 185–202.
- Ganguly, S., Samanta, A., Schull, M.A., Shabanov, N. V., Milesi, C., Nemani, R. R., et al. (2008). Generating vegetation leaf area index Earth system data record from multiple sensors. Part 2: Implementation, analysis and validation. *Remote Sensing of Environment*, 112(12), 4318–4332.
- Ganguly, S., Schull, M.A., Samanta, A., Shabanov, N. V., Milesi, C., Nemani, R. R., et al. (2008). Generating vegetation leaf area index earth system data record from multiple sensors. Part 1: Theory. *Remote Sensing of Environment*, 112(12), 4333–4343.
- Gesch, D. B. (2007). The national elevation dataset. In D. Maune (Ed.), *Digital elevation model technologies and applications: The DEM Users Manual* (2nd ed.) (pp. 99–118). Maryland, USA: American Society for Photogrammetry and Remote Sensing; Bethesda.
- Gibbs, H. K., Brown, S., Niles, J. O., & Foley, J. A. (2007). Monitoring and estimating tropical forest carbon stocks: Making REDD a reality. *Environmental Research Letters*, 2, 045023.
- Goetz, S. J., Baccini, A., Laporte, N. T., Johns, T., Walker, W., Kellndorfer, J., et al. (2009). Mapping and monitoring carbon stocks with satellite observations: A comparison of methods. *Carbon Balance and Management*, 4(2).
- Gurney, K. R., & Raymond, L. (2008). Targeting deforestation rates in climate change policy: A "Preservation Pathway" approach. *Carbon Balance and Management*, 3, 2.
- Gutman, G., Byrnes, R., Masek, J., Covington, S., Justice, C., Franks, S., & Headley, R. (2008). Towards monitoring land–cover and land–use changes at a global scale: The Global Land Survey 2005. *Photogrammetric Engineering and Remote Sensing*, 74, 6–10.
- Gutman, G., Huang, C., Chandler, G., Noojipady, P., & Masek, J. G. (2013). Assessment of the NASA-USGS Global Land Survey (GLS) datasets. *Remote Sensing of Environment*, 134, 249–265.
- Harding, D. J., & Carabajal, C. C. (2005). ICESat waveform measurements of within-footprint topographic relief and vegetation vertical structure. *Geophysical Research Letters*, 32, L21S10.
- Heath, L. S., Hansen, M., Smith, J. E., Miles, P. D., & Smith, B. W. (2008). Investigation into calculating tree biomass and carbon in the FIADB using a biomass expansion factor approach. In W. H. McWilliams, G. G. Moisen, & R. L. Czaplewski (Eds.), .
- Heuvelink, G. B.M. (1999). Propagation of error in spatial modelling with GIS. *Geographical information systems*, 1, 207–217.
- Hodgson, M. E., Jensen, J., Raber, G., Tullis, J., Davis, B.A., Thompson, G., et al. (2005). An evaluation of lidar-derived elevation and terrain slope in leaf-off conditions. *Photogrammetric engineering and remote sensing*, 71(7), 817.
- Houghton, R. A. (2005). Tropical deforestation as a source of greenhouse gas emissions. *Tropical deforestation and climate change*, 13.
- IPCC, C. C. (2007). The Physical Science Basis. *Contribution of Working Group I to the Fourth Assessment Report of the Intergovernmental Panel on Climate Change* (pp. 996). Cambridge, United Kingdom and New York, NY, USA: Cambridge University Press.
- Jenkins, J. C., Chojnacky, D. C., Heath, L. S., & Birdsey, R. A. (2003). National-scale biomass estimators for United States tree species. *Forest Science*, 49(1), 12–35.
- Kaufman, Y. J., Wald, A. E., Remer, L. A., Gao, B. C., Li, R. R., & Flynn, L. (1997). The MODIS 2.1- μ m channel-correlation with visible reflectance for use in remote sensing of aerosol. *Geoscience and Remote Sensing, IEEE Transactions on*, 35(5), 1286–1298.
- Keith, H., Mackey, B., Berry, S., Lindenmayer, D., & Gibbons, P. (2010). Estimating carbon carrying capacity in natural forest ecosystems across heterogeneous landscapes: Addressing sources of error. *Global Change Biology*, 16(11), 2971–2989.
- Kempes, C. P., West, G. B., Crowell, K., & Girvan, M. (2011). Predicting maximum tree heights and other traits from allometric scaling and resource limitations. *PLoS ONE*, 6(6), e20551.
- Lefsky, M.A. (2010). A global forest canopy height map from the moderate resolution imaging spectroradiometer and the geoscience laser altimeter system. *Geophysical Research Letters*, 37 (L15401).
- Lefsky, M.A., Harding, D., Cohen, W., Parker, G., & Shugart, H. (1999). Surface lidar remote sensing of basal area and biomass in deciduous forests of Eastern Maryland, USA. *Remote Sensing of Environment*, 67, 83–98.
- Lefsky, M.A., Harding, D. J., Keller, M., Cohen, W. B., Carabajal, C. C., Espirito-Santo, F. D. B., et al. (2005). Estimates of forest canopy height and aboveground biomass using ICESat. *Geophysical Research Letters*, 32(22) (L22S02).
- Lefsky, M.A., Keller, M., Pang, Y., De Camargo, P. B., & Hunter, M.O. (2007). Revised method for forest canopy height estimation from Geoscience Laser Altimeter System waveforms. *Journal of Applied Remote Sensing*, 1(1) 013537–013537.
- Lu, D. (2006). The potential and challenge of remote sensing-based biomass estimation. *International journal of remote sensing*, 27(7), 1297–1328.
- Lu, D., Chen, Q., Wang, G., Moran, E., Batistella, M., Zhang, M., et al. (2012). Aboveground forest biomass estimation with Landsat and LiDAR data and uncertainty analysis of the estimates. *International Journal of Forestry Research*, 16, <http://dx.doi.org/10.1155/2012/43653> (Article ID 436537).
- Masek, J. G., Vermote, E. F., Saleous, N. E., Wolfe, R., Hall, F. G., Huemmrich, K. F., et al. (2006). A Landsat surface reflectance dataset for North America, 1990–2000. *Geoscience and Remote Sensing Letters, IEEE*, 3(1), 68–72.
- McRoberts, R. E., Tomppo, E., Schadauer, K., Vidal, C., Stahl, G., Chirici, G., et al. (2009). Harmonizing national forest inventories. *Journal of Forestry*, 107(4), 179–187.
- Miles, L., & Kapos, V. (2008). Reducing greenhouse gas emissions from deforestation and forest degradation: Global land-use implications. *Science*, 320(5882), 1454–1455.
- Mitchard, E. T. A., Saatchi, S. S., Lewis, S. L., Feldpausch, T. R., Gerard, F. F., Woodhouse, I. H., et al. (2011). Comment on 'A first map of tropical Africa's above-ground biomass derived from satellite imagery'. *Environmental Research Letters*, 6, 049001.
- Nelson, R., Short, A., & Valenti, M. (2004). Measuring biomass and carbon in Delaware using an airborne profiling LIDAR. *Scandinavian Journal of Forest Research*, 19(6), 500–511.
- Niklas, K. J., & Spatz, H. -C. (2006). Allometric theory and the mechanical stability of large trees: Proof and conjecture. *American Journal of Botany*, 93(6), 824–828.
- Oksanen, J., & Sarjakoski, T. (2005). Error propagation of DEM-based surface derivatives. *Computers & Geosciences*, 31(8), 1015–1027.
- Pflugmacher, D., Cohen, W., Kennedy, R., & Lefsky, M. (2008). Regional applicability of forest height and aboveground biomass models for the Geoscience Laser Altimeter System. *Forest Science*, 54(6), 647–657.
- Saatchi, S., Sassan, Harris, N. L., Brown, S., Lefsky, M., Mitchard, E. T. A., et al. (2011). Benchmark map of forest carbon stocks in tropical regions across three continents. *Proceedings of the National Academy of Sciences*, 108(24), 9899–9904.
- Saatchi, S. S., Houghton, R. A., Dos Santos Alvalá, R. C., Soares, J. V., & Yu, Y. (2007). Distribution of aboveground live biomass in the Amazon basin. *Global Change Biology*, 13(4), 816–837.
- Saatchi, S., Marlier, M., Chazdon, R. L., Clark, D. B., & Russell, A. E. (2011). Impact of spatial variability of tropical forest structure on radar estimation of aboveground biomass. *Remote Sensing of Environment*, 115(11), 2836–2849.
- Shi, Y., Choi, S., Ni, X., Ganguly, S., Zhang, G., Duong, H. V., et al. (2013). Allometric scaling and resource limitations model of tree heights: Part 1. Model optimization and testing over continental USA. *Remote Sensing*, 5(1), 284–306.
- Stehman, S. V. (2009). Sampling designs for accuracy assessment of land cover. *International Journal of Remote Sensing*, 30(20), 5243–5272.
- Steininger, M. K. (2000). Satellite estimation of tropical secondary forest above-ground biomass: Data from Brazil and Bolivia. *International Journal of Remote Sensing*, 21(6–7), 1139–1157.
- Sun, G., Ranson, K. J., Kimes, D. S., Blair, J. B., & Kovacs, K. (2008). Forest vertical structure from GLAS: An evaluation using LVIS and SRTM data. *Remote Sensing of Environment*, 112(1), 107–117.
- West, G. B., Brown, J. H., & Enquist, B. J. (1999). A general model for the structure and allometry of plant vascular systems. *Nature*, 400(6745), 664–667.
- Wickham, J.D., Stehman, S. V., Gass, L., Dewitz, J., Fry, J. A., & Wade, T. G. (2013). Accuracy assessment of NLCD 2006 land cover and impervious surface. *Remote Sensing of Environment*, 130, 294–304.
- Wulder, M.A., White, J. C., Nelson, R. F., Næsset, E., Ørka, H. O., Coops, N. C., et al. (2012). Lidar sampling for large-area forest characterization: A review. *Remote Sensing of Environment*, 121, 196–209.
- Yang, W., Ni-Meister, W., & Lee, S. (2011). Assessment of the impacts of surface topography, off-nadir pointing and vegetation structure on vegetation lidar waveforms using an extended geometric optical and radiative transfer model. *Remote Sensing of Environment*, 115(11), 2810–2822.
- Zhang, X., & Kondragunta, S. (2006). Estimating forest biomass in the USA using generalized allometric models and MODIS land products. *Geophysical Research Letters*, 33(9) (L09402).

WWW1:http://www.mrlc.gov/nlcd_2006.php
 WWW2:http://svinetf4.fs.fed.us/clearinghouse/other_resources/ecosubregions.html
 WWW3:http://landsat.usgs.gov/science_GLS2005.php
 WWW4:<http://apps.fs.fed.us/fiadb-downloads/datamart.html>
 WWW5:<http://apps.fs.fed.us/Evaliator/tmtribute.jsp>
 WWW6:<http://www.whrc.org/mapping/nbcd/index.html>
 WWW7:<http://www.landfire.gov/vegetation.php>
 WWW8:<http://fsgeodata.fs.fed.us/rastergateway/biomass/>